THE PHOTOCURRENT AND THE OPEN-CIRCUIT VOLTAGE OF A SILICON SOLAR CELL

F. PELANCHON*, P. MIALHE** and J. P. CHARLES

Centre d'Electronique de Montpellier, Université des Sciences et Techniques du Languedoc, Place E. Bataillon, 34006 Montpellier (France)

(Received September 28, 1988; accepted in revised form May 30, 1989)

Summary

A study of the influence of the structure parameters of a silicon solar cell on both photocurrent and open-circuit voltage was performed. Fundamental carrier transport processes and non-ideal effects were taken into account with the main constraint relation that assumes a description of the current–voltage characteristic. The major influence of the recombination mechanism, compared with the band gap narrowing effect, on the cell performance was displayed. The work reveals practical doping levels to be $10^{17.5}$ - $10^{18.5}$ cm^{-3} for the base and 10^{18} - $10^{19.5}$ cm^{-3} for the emitter of an n^+–p cell, from which other structure parameter values are not of crucial influence, in order to obtain high open-circuit voltage values together with high efficiency values, provided that the front surface of the cell is well passivated.

1. Introduction

High efficiency is the key to large-scale applicability of photovoltaic devices. In the last five years, basic research in the area of cell design, of material quality, of cell processing and modeling led to silicon cell efficiencies increasing from 14% to 22%.

In high performance actual silicon cells, the emitter region is made fairly thin (0.1 - 0.2 μm) of n^+ type formed by low energy ion implantation, the emitter surface is oxide passivated to reduce surface recombination, and grid contact recombination is lowered by reducing the metal to silicon contact area [1 - 3]. The optical design has been improved [4] by forming microgrooves on the cell surface which allows oblique penetration of pho-

*Permanent address: Centre de Documentation Universitaire Scientifique et Technique, CEDUST, B.P. 3929, Damas, Syrie.

**Permanent address: Institut Supérieur des Sciences Appliquées et de la Technologie, ISSAT, B.P. 7028, Damas, Syrie.

0379-6787/90/$3.50

tons. Short-circuit current densities of these cells are very close to the theoretical limit but open-circuit voltage values are still less than the radiative limit.

In a solar cell, non-ideal effects, *e.g.* high level injection and energy gap shrinkage, influence the cell performance. Band edge distortion, present in heavily doped material, affects recombination, diffusion and drift. The band narrowing mechanism increases the steady state excess carrier density so the recombination currents are increased and the measured open-circuit voltage values are lower than expected. Crystal imperfections and foreign elements act as recombination centers producing low carrier lifetime values.

Major works in cell efficiency have placed the emphasis on improving the open-circuit voltage V_{oc} for maximum efficiency. Several different limits on the open-circuit voltage of silicon solar cells have been postulated from theoretical results by using approximated local equations or the first-order single diode model.

A systematic theory of the open-circuit voltage of a p–n junction has been given by Parrot [5] who has calculated V_{oc} as a function of the carrier concentrations at the junction. By assuming an abrupt p–n junction and non-degenerate conditions, he found that the photovoltage saturates when the illumination level increases to high levels. The effect of band gap narrowing in the heavily doped layers has been introduced [6] by using an effective intrinsic carrier concentration; V_{oc} saturation values are shown to be determined by the doping densities of the heavily doped layers. A general expression for the photovoltage valid for the case of a degenerate semiconductor has been considered [7] by using the Landsberg diffusion–mobility relation [8]. Later de Visschere [9] generalized Parrot's theory to include degenerate carrier densities and heavy doping effect. In these works, the open-circuit voltage values depend on the *pn* product values without relationship to the illumination level.

V_{oc} has been related to internal potential differences [10] using an "effective" saturation current density J_d as a parameter. This method has been used [11 - 14] to describe the behavior of silicon solar cells in concentrated sunlight. A theory [15] based on the transport equation has been developed and applied to back-surface field (BSF) solar cells.

Weaver [16] performed exact numerical calculations (including band gap narrowing, Auger mechanism and non-uniform generation rate) to compare BSF solar cells with conventional cells.

Numerous published studies consider that V_{oc} may be expressed by the well known equation

$$V_{oc} = (KT/q) \ln(I_{ph}/I_0) + 1 \tag{1}$$

where I_{ph} is the photocurrent density and I_0 the dark reverse saturation current density. The solar cell is modeled with a constant current source I_{ph} in parallel with an ideal diode. The open-circuit voltage appears as a function of intrinsic parameters. Many results [17 - 21] have been obtained in this manner. This approach ignores the fact that eqn. (1) is not valid for discussing

the effect of recombination since it supposes an ideal diode with a quality factor which equals unity.

All these studies lead to theoretical values of V_{oc} less than the radiative limit or show limitations when optimizing structure parameters or when increasing the illumination level. Such results are attributed to recombination processes in the bulk of the cell or to the high surface recombination velocity of the metal–electrode interfaces, but this has not been shown by the theory. All the theories developed have assumed that the recombination current in the space-charge region is negligible and have considered a parameter, the surface recombination velocity, which is shown to take suitable values in order to explain desired results. So discrepancies between theory and experiment are attributed to approximations made in order to obtain manageable equations.

The analysis of solar cell performances must take into account non-ideal effects, *e.g.* high level injection, energy gap shrinkage, and recombination processes in the bulk, in the space-charge region and at the metal electrode interface, to obtain a description of the current–voltage characteristics. It is not correct to consider a structure with a cell design which has been optimized for operation in the open-circuit condition as giving the best efficiency. Experimental, theoretical and modeling studies of V_{oc} are interesting because they reveal information about fundamental mechanisms operating in the layers of the cells.

In this study of solar cell performances, fundamental processes (drift, diffusion, recombination, creation), non-ideal effects and cell design are taken into account in order to obtain a description of the current–voltage characteristics. The influences of physical mechanisms and of structure parameters on the photocurrent, the open-circuit voltage and the maximum output power are pointed out and optimum values are given.

2. Theory and discussion

Modeling studies [22 - 24] have shown that the current–voltage relation

$$f(I, V) = 0 \tag{2}$$

with

$$f(I, V) = I_{ph} - \sum_{i=1,2} I_{0i}\{\exp(B_i V_d) - 1\} - V_d/R_{sh} \tag{3}$$

where $V_d = V + IR_s$, $B_1 = q/KT$ and $B_2 = B_1/2$, is adequate to represent experimental data.

I_{01} is the dark saturation current which results from electronic conduction phenomena in the quasi-neutral regions of the cell (diffusion, recombination, including the drift effect), and I_{02} is the excess current which may

result from a variety of causes. Recombination in the space-charge region and via deep levels [14, 25 - 27] or at a metal–semiconductor contact [28] are well known as causes of this behavior with a diode quality factor equal to 2. Current-proportional voltage is described by a lumped series resistance R_s and leakage currents are expressed by the addition of a lumped shunt resistance R_{sh}.

The photocurrent I_{ph} depends on two kinds of factors: (1) factors associated with internal structural properties of the solar cell, such as the dopant concentrations N_A and N_D, the surface recombination velocities S_F (front surface) and S_B (back surface), and the widths of the three parts, emitter (X), space charge (W) and base (H) regions of the cell; (2) the incident photon flux $F(\lambda)$ and absorption capacity of silicon $A(\lambda)$. Expressions of the contributions to the photocurrent from these three regions respectively $J_p(\lambda)$, $J_n(\lambda)$, $J_{dr}(\lambda)$ as functions of parameters X, W, H, S_F, S_B, diffusion lengths $L_p(L_n)$, diffusion coefficients $D_p(D_n)$, and $A(\lambda)$, $F(\lambda)$ are given by eqns. (15), (19) and (20) of ref. 29. I_{ph} is obtained by integrating the expressions of monochromatic currents from $\lambda = 0.24$ μm to $\lambda = 1.08$ μm (useful bandwidth for silicon); the experimental values of $F(\lambda)$ and $A(\lambda)$ (AM 1 conditions) may be fitted with five linear curves (see Appendix 1). Some authors [21, 30, 31] used the generation rate of electron–hole pairs to calculate the observed short-circuit current as an approximation of I_{ph}.

The reverse saturation current I_{01} (first diode in the model) is the classical diffusion–recombination current from the emitter and the base of the cell, taking into account the energy band gap narrowing [32] whose importance has been shown [17, 33].

The model of the solar cell adopted is that of an abrupt junction with homogeneously doped sides and it leads to the dark saturation current given by the following expression [29]

$$I_{01} = I_{0E} + I_{0B} \tag{4}$$

with

$$I_{0B} = q(n_i^2/N_A)\,(D_n/\tau_n)^{1/2} A/B \tag{5}$$

$$I_{0E} = q(n_i^2/N_D)(D_p/\tau_p)^{1/2} C/D \tag{6}$$

and

$$A = (S_F L_p/D_p)\cosh(X/L_p) + \sinh(X/L_p) \tag{7}$$

$$B = (S_F L_p/D_p)\sinh(X/L_p) + \cosh(X/L_p) \tag{8}$$

$$C = (S_B L_n/D_n)\cosh(H/L_n) + \sinh(H/L_n) \tag{9}$$

$$D = (S_B L_n/D_n)\sinh(H/L_n) + \cosh(H/L_n) \tag{10}$$

where the intrinsic carrier concentration n_i is replaced by the effective intrinsic concentration to take into account the energy band gap narrowing

[21, 32], and τ_n (τ_p) is the electron (hole) lifetime in the base (emitter) region. Equation (4) gives $I_{0\,1}$ as the sum of two terms, a base current $I_{0\,B}$ and an emitter current $I_{0\,E}$. Fossum *et al.* [17] have shown the emitter to be transparent to minority carriers when $S_F \ll 10^2$ cm s^{-1} and when the required transit time for minority carriers to cross the emitter is lower than the average minority carrier lifetime τ_p, which leads to the dominance of the base current in eqn. (4). Such results have been confirmed by Shibib and Fossum [18] who provided data taken on BSF silicon solar cells. $I_{0\,2}$ is the total recombination current of electrons and holes including the space-charge region [26].

In this work, the doping concentrations N_A and N_D vary in their usual ranges for actual silicon solar cells, 10^{15} $10^{18.5}$ cm^{-3} for N_A and 10^{18} 10^{21} cm^{-3} for N_D. So the Auger effect may be neglected in the base and has to be considered in the emitter; in these two cases, the lifetimes τ_n and τ_p and the diffusion coefficients are known [31] as functions of N_A and N_D, and the diffusion length can be computed by the relations $L = (\tau D)^{1/2}$. In this way, the reverse saturation currents I_{0i} and the photocurrent I_{ph} are related to the structure parameters N_A, N_D, X, H, S_F, S_B. This model allows the description of cell performance with structure parameters taking into account the true value of the photocurrent when varying the cell structure or the illumination level.

The open-circuit voltage V_{oc}, deduced from eqn. 3 by making $I = 0$, is the solution of the implicit equation

$$I_{ph} - V_{oc}/R_{sh} - \sum_{i=1,2} I_{0i}\{\exp(B_i V_{oc}) - 1\} = 0 \tag{11}$$

The lumped shunt resistance value can be taken as equal to 1000 Ω cm^2 [33] which is in good agreement with actual solar cells. For the maximum output power of Fig. 12, the series resistance R_s is taken equal to 0.1 Ω cm^2 [33].

3. Results

3.1. Influence of intrinsic parameters on I_{ph}

Figures 1(a), (b) and (c) display the emitter, the space-charge and the base cumulative photocurrent values when increasing the absorbed photon wavelength. Photons with wavelength values less than 0.49 μm are absorbed by the emitter and contribute to the emitter photocurrent. A great amount of those photons of wavelengths more than 0.49 μm are absorbed by the two other regions and contribute to these two region photocurrents. The space-charge current shows a strong dependency on both the base doping level N_A and the emitter doping level N_D.

3.2. Influence of structure parameters on I_{ph}

To study the photocurrent I_{ph}, the base width H and the back-surface recombination velocity S_B are taken to be greater than 80 μm and 10^5 cm s^{-1} respectively. A strong dependency of the total photocurrent on the

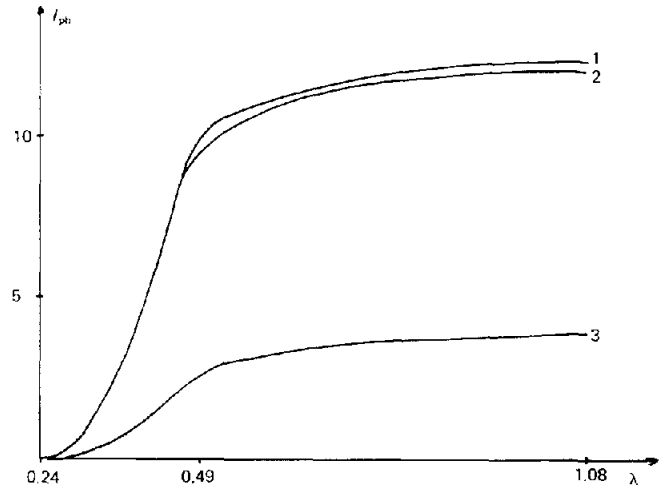

(a)

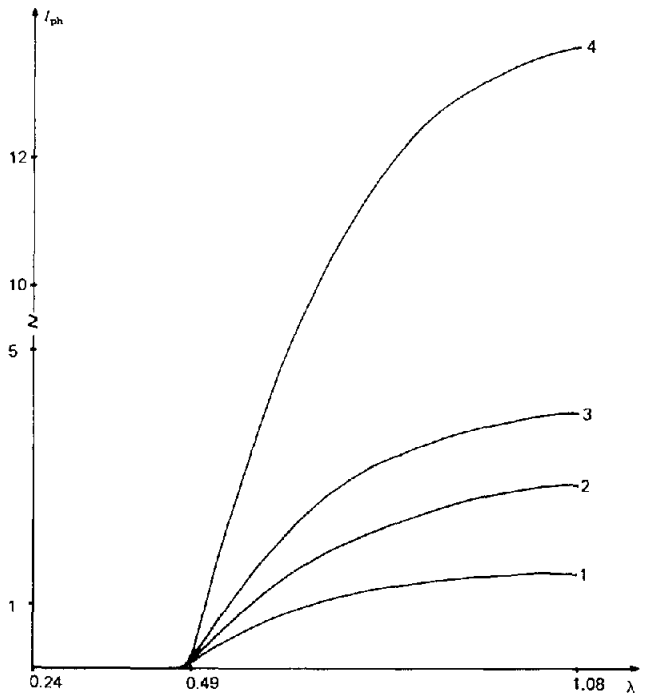

(b)

Fig. 1. *(continued)*

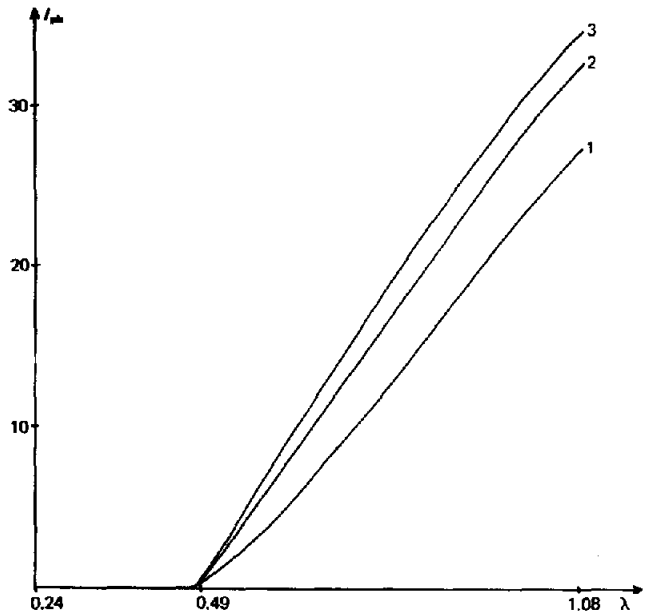

(c)

Fig. 1. (a) Cumulative emitter photocurrent I_{ph} (mA cm^{-2}) *vs.* photon wavelength λ (μm) for $X = 0.1$ μm, $S_F = 100$ cm s^{-1}: for curves 1, 2 and 3, N_D is 10^{19}, 10^{20} and 10^{21} cm^{-3} respectively. (b) Cumulative space-charge photocurrent I_{ph} (mA cm^{-2}) *vs.* photon wavelength λ (μm) for $X = 0.1$ μm, $S_F = 100$ cm s^{-1}: curve 1, $N_A = 10^{17}$ cm^{-3}, $N_D = 10^{20}$ cm^{-3}; curve 2, $N_A = 10^{16}$ cm^{-3}, $N_D = 10^{20}$ cm^{-3}; curve 3, $N_A = 10^{15}$ cm^{-3}, $N_D = 10^{20}$ cm^{-3}; curve 4, $N_A = 10^{16.5}$ cm^{-3}, $N_D = 10^{17.5}$ cm^{-3}. (c) Cumulative base photocurrent I_{ph} (mA cm^{-2}) *vs.* photon wavelength λ (μm) for $N_D = 10^{20}$ cm^{-3}, $X = 0.1$ μm, $H = 295$ μm, $S_F = 100$ cm s^{-1}, $S_B = 10^{15}$ cm s^{-1}: for curves 1, 2 and 3, N_A is 10^{15}, 10^{16} and 10^{17} cm^{-3} respectively.

emitter width appears on curves A, B and E in Fig. 2. It shows the generally postulated results concerning the need of a small emitter width for practical emitter and base doping levels and for front-surface recombination velocity S_F lower than 100 cm s^{-1} in order to obtain high I_{ph} values. In the case of parameter (N_A, N_D, S_F) values giving large V_{oc} values (see below), the total photocurrent does not depend on an emitter width lower than 1 μm (Fig. 2, curve C) which is an important result for cell design.

We obtain no significant dependency of I_{ph} on the base width when H is greater than 80 μm and this result is in agreement with classical short-circuit current studies [29]. Figure 3 shows a strong dependency of the emitter photocurrent on the front-surface recombination velocity S_F as soon as S_F is strong enough to recombine the created electron–hole pairs before they can contribute to the photocurrent. For large N_D values, the influence of S_F is smaller but the photocurrent is considerably reduced. When the back-surface recombination velocity S_B is greater than 10^5 cm s^{-1}, I_{ph} does not depend on S_B. A systematic representation of the emitter and base doping effects on the photocurrent are displayed in Figs. 4, 5, 6 and 7. The

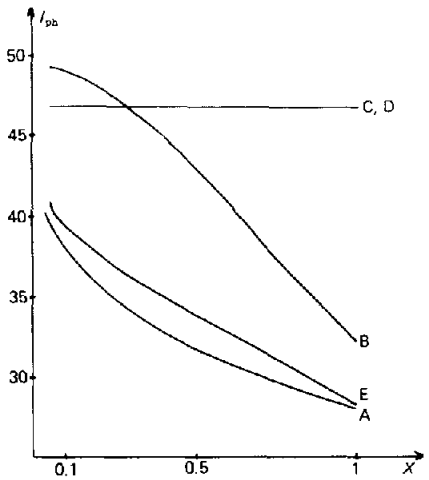

Fig. 2. Total photocurrent I_{ph} (mA cm^{-2}) *vs.* emitter width X (μm): curves A and B, $N_A = 10^{16.5}$ cm^{-3}, $N_D = 10^{20}$ cm^{-3}, $H = 295$ μm, $S_B = 10^{15}$ cm s^{-1}; curve A, $S_F = 10^7$ cm s^{-1}; curve B, $S_F = 100$ cm s^{-1}; curve C, $N_A = 10^{17.7}$ cm^{-3}, $N_D = 10^{18.8}$ cm^{-3}, $H = 295$ μm, $S_F = 100$ cm s^{-1}, $S_B = 10^{15}$ cm s^{-1}; curve D, N_A, N_D, S_B as for curve C, $H = 100$ μm, $S_F = 0.01$ cm s^{-1}; curve E, N_A, N_D, H, S_B as for curve D, $S_F = 10^6$ cm s^{-1}.

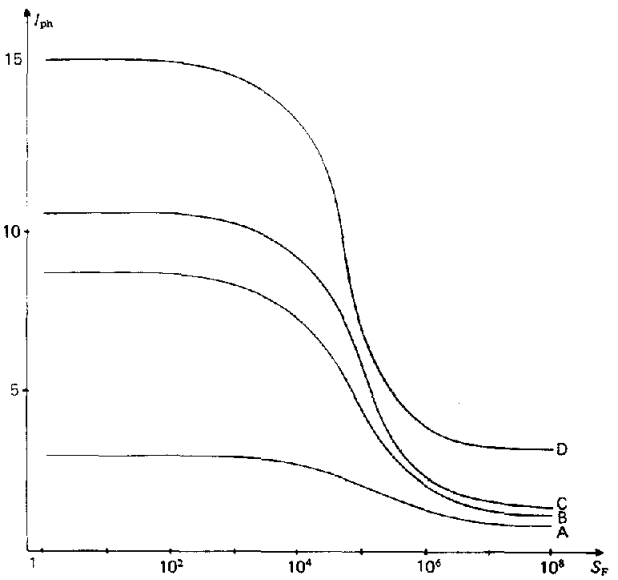

Fig. 3. Emitter photocurrent I_{ph} (mA cm^{-2}) *vs.* front-surface recombination velocity S_F (cm s^{-1}): for curves A, B and C, $X = 0.1$ μm, N_D is 10^{21}, 10^{20} and 10^{19} cm^{-3} respectively; curve D, $X = 0.3$ μm, $N_D = 10^{18.9}$ cm^{-3}.

emitter photocurrent strongly decreases when N_D increases beyond 10^{20} cm^{-3} and is nearly insensitive to N_D values less than 10^{20} cm^{-3}. When the emitter is highly doped, the minority carrier lifetime strongly decreases because of the increase in the band-to-band Auger recombination. Figure 5

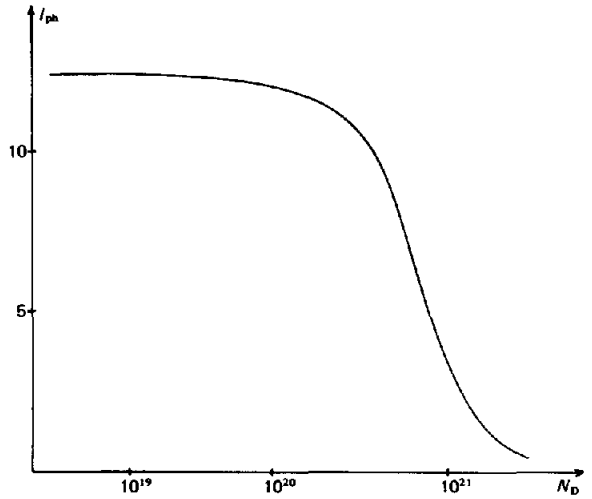

Fig. 4. Emitter photocurrent I_{ph} (mA cm^{-2}) *vs.* emitter doping N_D (cm^{-3}): X = 0.1 μm, S_F = 100 cm s^{-1}.

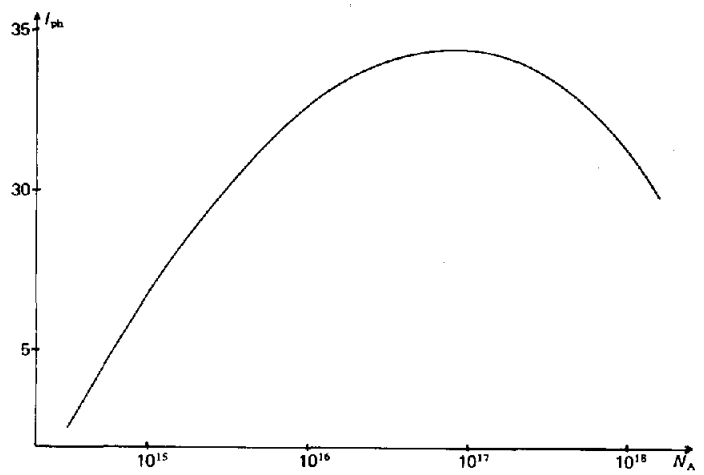

Fig. 5. Base photocurrent I_{ph} (mA cm^{-2}) *vs.* base doping N_A (cm^{-3}): N_D = 10^{20} cm^{-3}, X = 0.1 μm, H = 295 μm, S_F = 100 cm s^{-1}, S_B = 10^{15} cm s^{-1}.

shows a maximum base photocurrent value for a base doping level around $N_A = 10^{17}$ cm^{-3}, which corresponds to an equilibrium between the increase in created electron–hole pairs and their recombination as diffusion length is lowered by the increase in doping. Figures 6 and 7 conclude this study with the displays of the photocurrent *vs.* the doping levels, taking into account the space-charge contribution, and indicating useful doping values for obtaining large values of the total photocurrent.

3.3 Influence of structure parameters on V_{oc}

The fundamental influence of the structure parameters on the open-circuit voltage has been previously placed in a prominent position and we

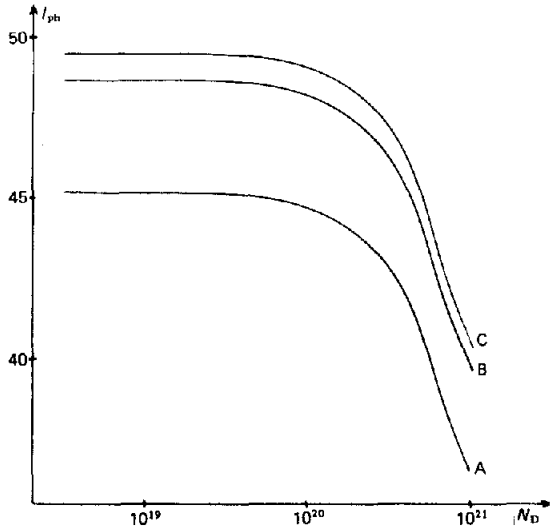

Fig. 6. Total photocurrent I_{ph} (mA cm^{-2}) *vs.* emitter doping N_D (cm^{-3}), $X = 0.1$ μm, $H = 295$ μm, $S_F = 100$ cm s^{-1}, $S_B = 10^{15}$ cm s^{-1}: for curves A, B and C, N_A is 10^{18}, 10^{17} and 10^{16} cm^{-3} respectively.

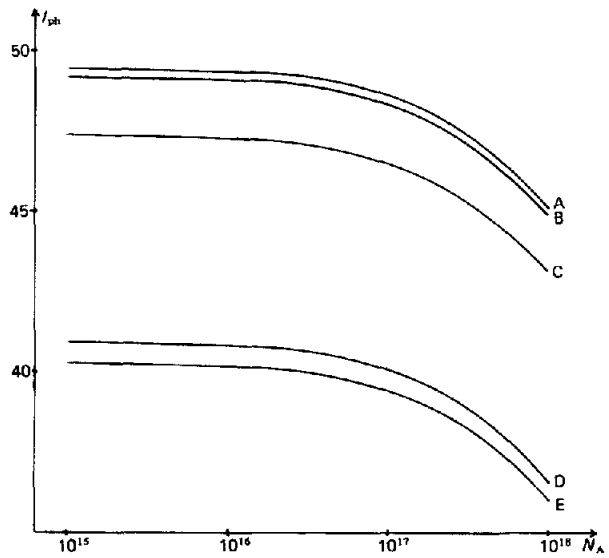

Fig. 7. Total photocurrent I_{ph} (mA cm^{-2}) *vs.* base doping N_A (cm^{-3}): for curves A–E, N_D is 10^{19}, 10^{20}, $10^{20.5}$, 10^{21} and 10^{19} cm^{-3} respectively, $X = 0.1$ μm, $H = 295$ μm, $S_B = 10^{15}$ cm s^{-1}; curves A–D, $S_F = 100$ cm s^{-1}; curve E, $S_F = 10^6$ cm s^{-1}.

study first the dependence of V_{oc} on the emitter width X for the same S_F values as for I_{ph} (see Fig. 8). For small X values, lower than 0.3 μm, V_{oc} is strongly dependent on S_F; curves A and B in Fig. 8 compared with curves A and B in Fig. 2 illustrate that V_{oc} is limited by front-surface recombination. As X increases, V_{oc} becomes less sensitive to S_F and its decrease results

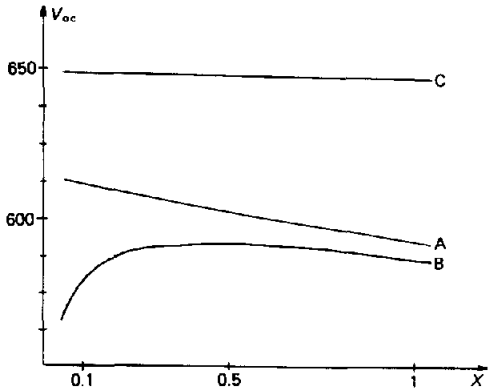

Fig. 8. Open-circuit voltage V_{oc} (mV) *vs.* emitter width X (μm): curves A and C, H = 295 μm, S_F = 100 cm s^{-1}, S_B = 10^5 cm s^{-1}; curves A and B, N_D = 10^{20} cm^{-3}, N_A = $10^{16.5}$ cm^{-3}; curve B, H = 295 μm, S_F = 10^7 cm s^{-1}; curve C, N_D = 10^{19} cm^{-3}, N_A = $10^{17.7}$ cm^{-3}.

from the emitter photocurrent decrease, observed in Fig. 2. This is explained by the fact that the emitter width becomes larger than the diffusion length, (confirmed by curve C of Fig. 8) obtained for lower doping values (then higher diffusion lengths) chosen to lead to optimum V_{oc} values (see below). This constitutes an important result since curve C in Fig. 8 shows V_{oc} is insensitive to the emitter width (lower than 1 μm) for some structure parameter values. Curve B in Fig. 9 shows that in the case of doping levels considered for optimum open- circuit voltage values, the front-surface recombination velocity influence on V_{oc} is stronger than for the case of larger doping values leading to reduced V_{oc} values. For low S_F values (less than 10^3 cm s^{-1}) V_{oc} is insensitive to S_F. This result is correlated to the previously discussed photocurrent curve Fig. 3; moreover, the diffusion current due to the emitter I_{0E} remains negligible compared with the base contribution I_{0B}. This is no longer true when S_F increases beyond 10^3 cm s^{-1}.

Such results display the comparative contributions to recombination from the surface effect and from the Auger effect which strongly increases

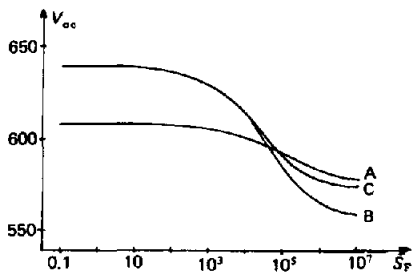

Fig. 9. Open-circuit voltage V_{oc} (mV) *vs.* front-surface velocity S_F (cm s^{-1}), S_B = 10^{15} cm s^{-1}: curve A, N_D = 10^{20} cm^{-3}, N_A = $10^{16.5}$ cm^{-3}, X = 0.1 μm, H = 295 μm; curve B, N_D = 10^{19} cm^{-3}, N_A = $10^{17.7}$ cm^{-3}, X = 0.1 μm, H = 160 μm; curve C, N_D = 10^{19} cm^{-3}, N_A = $10^{17.7}$ cm^{-3}, H = 160 μm, X = 0.2 μm.

with doping levels higher than 10^{19} cm^{-3}. These are pointed out in Fig. 10 with the variations of calculated V_{oc} values *vs.* emitter doping level N_D for two different S_F values. V_{oc} is very dependent on N_D when S_F is high and is nearly constant when S_F is low. We have shown that these variations, previously observed [34 - 36], are a result of photocurrent behavior and put the stress on the importance of front-surface passivation. With an efficient passivation, a low emitter doping level around 10^{18} - $10^{19.5}$ cm^{-3} is enough to obtain large V_{oc} values. Figures 11 and 12 display the variations of V_{oc} against the base doping level for usual N_D values. The curves in Fig. 11 show that larger V_{oc} values are obtained in the base doping range $10^{17.5}$ - $10^{18.5}$ cm^{-3} regardless of the other parameters; the slight difference to the results in ref. 16 is due to the consideration of the space-charge contribution we used. These results may explain the flatter and the larger V_{oc} maximum value range in Fig. 11 compared with previous results [16]. The influence of band gap narrowing appears clearly in Fig. 12; V_{oc} is nearly saturating around $N_A = 10^{17}$ cm^{-3} and decreases beyond $N_A = 10^{18}$ cm^{-3}.

In the case of I_{ph}, no dependency of V_{oc} on the base width and the back-surface recombination velocity occurs provided that H and S_B are greater than 80 μm and 10^5 cm s^{-1} respectively. Although not shown graphically, our model predicts higher values of the open-circuit voltage when relatively low values of the base width and the back-surface recombination velocity are assigned. For instance, we obtained $V_{oc} = 690$ mV with $N_D = 10^{18.5}$ cm^{-3}, $N_A = 10^{17}$ cm ^{3}, $X = 0.2$ μm, $H = 10$ μm, $S_F = 1$ cm s^{-1} and $S_B = 1$ cm s^{-1}. In this structure, the minority carrier diffusion length in the base is greater than the base width which improves the collection of carriers.

Curve C of Fig. 12 illustrates an application of the model to the determination of the maximum output power P_M; the existence of an optimum base doping level was known [21] and it is of importance to note that optimum I_{ph}, V_{oc} and P_M values are obtained for different values of structure parameters.

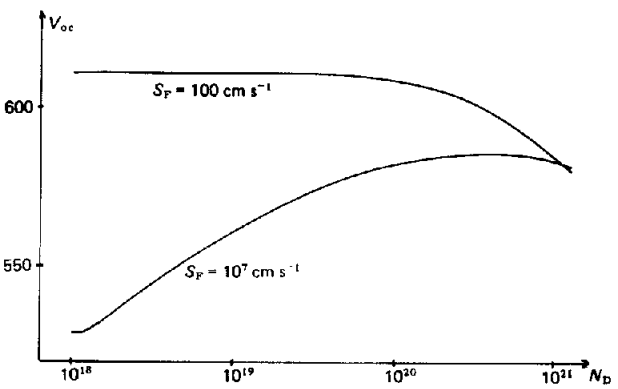

Fig. 10. Open-circuit voltage V_{oc} (mV) *vs.* emitter doping N_D (cm^{-3}): $N_A = 10^{16.5}$ cm^{-3}, $X = 0.1$ μm, $H = 295$ μm, $S_B = 10^{15}$ cm^{-3}.

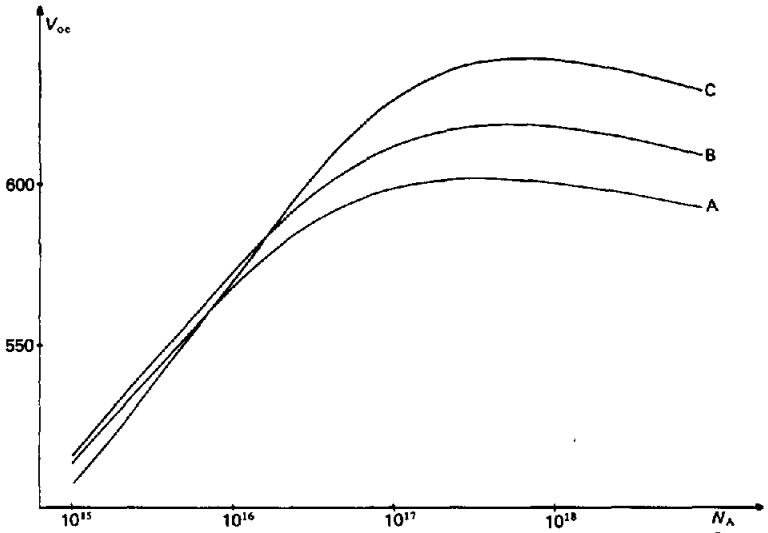

Fig. 11. Open-circuit voltage V_{oc} (mV) *vs.* base doping N_A (cm^{-3}): curves A–C, H = 295 μm, $S_B = 10^{15}$ cm s^{-1}; curve A, $N_D = 10^{20}$ cm^{-3}, X = 0.2 μm, $S_F = 10^6$ cm s^{-1}; curve B, $N_D = 10^{20}$ cm^{-3}, X = 0.6 μm, S_F = 100 cm s^{-1}; curve C, $N_D = 10^{18.5}$ cm^{-3}, X = 0.05 μm, S_F = 2 cm s^{-1}.

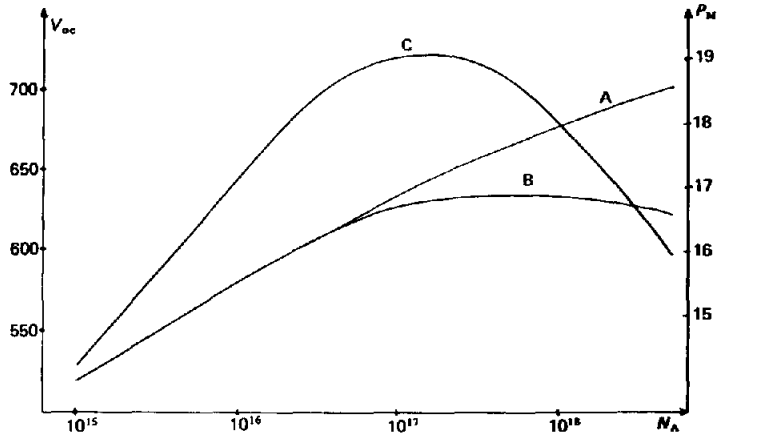

Fig. 12. Curves A and B, open-circuit voltage V_{oc} (mV) *vs.* base doping N_A (cm^{-3}): curve A, with band gap narrowing; curve B, without band gap narrowing. Curve C, maximum output power P_M (mW cm^{-2}) *vs.* N_A with band gap narrowing, $N_D = 10^{20}$ cm^{-3}, X = 0.1 μm, H = 295 μm, S_F = 100 cm s^{-1}, $S_B = 10^{20}$ cm s^{-1}.

4. Conclusion

A systematic study of the influence of the structure parameters of a solar cell on both photocurrent and open-circuit voltage has been performed. Non-ideal effects and recombination processes have been taken into account by using a double-diode description of the current–voltage characteristics. In this way, actual cell structures are considered with constraint relations

between measurable characteristics. Our calculations reveal efficient doping level ranges, for the base ($10^{17.5}$ - $10^{18.5}$ cm^{-3}) and for the emitter (10^{18} - $10^{19.5}$ cm^{-3}), where geometrical structure parameter values (emitter and base widths, back-surface recombination velocity) are not of crucial importance in obtaining high V_{oc} values. However, in the case of thin emitter region, the important lowering of V_{oc} values because of high front-surface recombination velocity is shown. The major influence on the cell performances of the recombination mechanism compared with the band gap narrowing effect has been displayed. It is also pointed out that large photocurrent, open-circuit voltage and maximum output power are not obtained for the same parameter values. This constitutes an important result and alters some preconceptions.

Appendix

The experimental curves given for $A(\lambda)$ and $F(\lambda)$ by Hovel [29] are valid in 100 Å bandwidths. In our model, they are fitted with five linear curves

$$0.24\ \mu m \leqslant \lambda \leqslant 0.29\ \mu m \qquad A(\lambda) = -806\,000/\lambda + 6\,590\,000\ cm^{-1} \qquad (12)$$

$$0.30\ \mu m \leqslant \lambda \leqslant 0.49\ \mu m \qquad A(\lambda) = 2\,614\,000/\lambda - 5\,244\,000\ cm^{-1} \qquad (13)$$

$$0.50\ \mu m \leqslant \lambda \leqslant 1.08\ \mu m \qquad A(\lambda) = 11\,658/\lambda - 10\,385\ cm^{-1} \qquad (14)$$

and

$$0.24\ \mu m\ \lambda \leqslant 0.47\ \mu m \qquad F(\lambda) = (21.7\lambda - 5.21)10^{15}/cm^2\ s^{-1} \qquad (15)$$

$$0.48\ \mu m \leqslant \lambda \leqslant 1.08\ \mu m \qquad F(\lambda) = (-2.74\lambda + 6.29)10^{15}/cm^2\ s^{-1} \qquad (16)$$

For every 100 Å bandwidth between 0.24 and 1.08 μm, the photocurrents generated in each region of the cell (J_n, J_{dr}, J_p) under AM 1 conditions are given by well known expressions [29] and the contributions (I_n, I_{dr}, I_p) for all absorbed wavelengths are computed by using eqns. 12 - 16; for example

$$I_n = \sum_{i=1\ \text{to}\ 85} J_n \qquad \{\lambda = 0.24 + 0.01(i-1)\} \qquad (17)$$

and the total photocurrent is

$$I_{ph} = I_n + I_{dr} + I_p \qquad (18)$$

References

1 M. A. Green, A. W. Blakers, J. Shi, E. M. Keller and S. Wenham, *IEEE Trans. Electron Devices, 31* (1984) 679 - 693.

2 K. W. Boer, *Sol. Wind Technol., 4* (1987) 21 - 35.

3 R. M. Swanson, S. K. Beckmith, R. A. Crane, W. O. Deades, Y. H. Kwark, R. A. Sinton and S. E. Swirhun, *IEEE Trans. Electron Devices, 31* (1984) 661 - 671.

4 A. W. Blakers and M. A. Green, *Appl. Phys. Lett., 48* (1986) 215 - 217.
5 J. E. Parrot, *IEEE Trans. Electron Devices, 21* (1974) 89 - 93.
6 C. Hu and C. Rowley, *Proc. 13th IEEE Photovoltaic Specialists' Conf., Washington, DC, 1978* IEEE, New York, 1978.
7 D. V. Kumar and S. K. Sharma, *Solid-State Electron., 25* (1982) 1161 - 1164.
8 P. T. Landsberg, *Proc. R. Soc. London, Ser. A, 213* (1952) 226 - 237.
9 P. de Visschere, *Solid-State Electron., 27* (1984) 131 - 136.
10 J. G. Fossum and F. A. Lindholm, *IEEE Trans. Electron Devices, 24* (1977) 325 - 329.
11 J. G. Fossum, E. L. Burgess and F. A. Lindholm, *Solid-State Electron., 21* (1978) 729 - 737.
12 C. Y. Wu and W. Z. Shen, *Solid-State Electron., 23* (1980) 209 - 216.
13 S. R. Dhariwal, L. S. Kothari and S. C. Jain, *IEEE Trans. Electron Devices, 23* (1976) 504 - 507.
14 R. N. Hall, *Solid-State Electron., 24* (1981) 595 - 616.
15 S. R. Dhariwal and A. P. Kulshreshtha, *Solid-State Electron., 24* (1981) 1161 - 1165.
16 H. T. Weaver, *Sol. Cells, 5* (1982) 275 - 292.
17 J. G. Fossum, A. Lindholm and M. Ayman Shibib, *IEEE Trans. Electron Devices, 26* (1979) 1294 - 1298.
18 M. Ayman Shibib and G. Fossum, *J. Appl. Phys., 52* (1981) 1072 - 1075.
19 M. A. Green, *IEEE Trans. Electron Devices, 31* (1984) 671 - 678.
20 O. von Roos and P. T. Landsberg, *J. Appl. Phys., 57* (1985) 4746 - 4751.
21 S. N. Mohammad, *J. Appl. Phys., 61* (1987) 767 - 772.
22 J. P. Charles, I. Mekkaoui-Alaoui, G. Bordure and P. Mialhe, *Rev. Phys. Appl., 19* (1984) 851 - 857.
23 J. P. Charles, I. Mekkaoui-Alaoui, G. Bordure and P. Mialhe, *Solid-State Electron., 28* (1985) 807 - 820.
24 G. L. Araujo, E. Sanchez and P. Marti, *Sol. Cells, 5* (1984) 199 - 204.
25 C. T. Sah, R. N. Noyce and W. Shockley, *Proc. IRE, 45* (1957) 1228 - 1243.
26 A. Nussbaum, *Phys. Status Solidi A, 19* (1973) 441 - 450, p. 444, eqn. 19.
27 M. Wolf, G. T. Noel and J. Stirn, *IEEE Trans. Electron Devices, 24* (1977) 419 - 428.
28 P. Panayotatos and H. C. Card, *Solid-State Electron., 23* (1980) 41 - 46.
29 H. J. Hovel, Solar Cells, in R. K. Willardson and A. C. Beer (eds.), *Semiconductors and Semimetals*, Vol. 11, Academic Press, New York, 1975.
30 H. Hsieh, C. Hu and C. I. Drowley, *IEEE Trans. Electron Devices, 27* (1980) 883 - 885.
31 M. J. Chen and C. Y. Wu, *Solid-State Electron., 28* (1985) 751 - 761.
32 J. W. Slotboom and H. C. de Graaf, *Solid-State Electron., 19* (1976) 857 - 862.
33 F. Pelanchon, P. Mialhe and P. Charles, *Rev. Phys. Appl., 23* (1988) 1139 - 1145.
34 P. Lauwers, J. van Meerbergen, P. Bulteel, R. Mertens and R. van Overstraeten, *Solid-State Electron., 21* (1978) 747 - 752.
35 S. N. Mohammad and S. T. H. Abidi, *J. Appl. Phys., 61* (1987) 4909 - 4919.
36 M. A. Shibib, F. A. Lindholm and J. G. Fossum, *IEEE Trans. Electron Devices, 26* (1979) 1104 - 1106.